CARBON 49 (2011) 5107–5116

available at www.sciencedirect.com

ScienceDirect

journal homepage: www.elsevier.com/locate/carbon

Thermal conductivity and structure of non-covalent functionalized graphene/epoxy composites

Chih-Chun Teng [a], Chen-Chi M. Ma [a,*], Chu-Hua Lu [b], Shin-Yi Yang [a], Shie-Heng Lee [a], Min-Chien Hsiao [a], Ming-Yu Yen [a], Kuo-Chan Chiou [c], Tzong-Ming Lee [c]

[a] Department of Chemical Engineering, National Tsing Hua University, Hsin-Chu 30043, Taiwan
[b] Department of Applied Chemistry, National Chiao Tung University, Hsin-Chu 30010, Taiwan
[c] Material and Chemical Research Laboratories, Industrial Technology Research Institute, Hsin-Chu 31040, Taiwan

ARTICLE INFO

Article history:
Received 24 January 2011
Accepted 24 June 2011
Available online 23 July 2011

ABSTRACT

Non-covalent functionalization was used to functionalize graphene nanosheets (GNSs) through π–π stacking of pyrene molecules with a functional segmented polymer chain, which results in a remarkable improvement in the thermal conductivity of GNS-filled polymer composites. The functional segmented poly(glycidyl methacrylate) containing localized pyrene groups (Py-PGMA) was prepared by atom transfer radical polymerization, and Py-PGMA was characterized by nuclear magnetic resonance spectroscopy. Raman spectra, X-ray photoelectron spectroscopy and thermogravimetric analysis reveal the characteristics of Py-PGMA–GNS. Differential scanning calorimetry indicated that the functional groups on Py-PGMA–GNSs can generate covalent bonds with the epoxy matrix, and further form a cross-linked structure in Py-PGMA–GNS/epoxy composites. The Py-PGMA on the GNS surface not only plays an important role to facilitate a homogeneous dispersion in the polymer matrix but also improves the GNS–polymer interaction, which results in a high contact area. Consequently, the thermal conductivity of integrated Py-PGMA–GNS/epoxy composites exhibited a remarkable improvement and is much higher than epoxy reinforced by multi-walled carbon nanotubes or GNSs. The thermal conductivity of 4 phr Py-PGMA–GNS/epoxy has about 20% (higher than that of pristine GNS/epoxy) and 267% (higher than pristine MWCNT/epoxy).

1. Introduction

Polymer composites with carbon nanofillers have many potential applications, including thermal management, electronics, green energies, and transportation [1]. With the growing demand for high density electronic devices, developing polymer-based composites with high thermal conductivity and low fabrication cost is of primary importance. On the basis of previous investigation on polymer-based composites, polymers filled with thermally conductive particles such as alumina [4], boron nitride [5], and alumina nitride [6] are conventional to enhance the performance of polymer composites. However, they relied on excessively high quantity of fillers (about 30–60 vol%) to achieve thermal conductivity values of 1–2 W/mK. Carbon-based nanofillers, such as carbon nanotubes and carbon nanofibers, possess unique nanostructures, high aspect ratio, and superior thermal conductivity, they were expected to be the potential fillers for improving the thermal conductivity of polymer composites [7–9]. However, there are two main reasons limiting the applications of polymer composites with carbon nanofillers: (1) the poor dispersion of carbon nanofillers in polymeric matrices, which limited the

* *Corresponding author:* Fax: +886 3 571 5408.
E-mail address: ccma@che.nthu.edu.tw (Chen-Chi M. Ma).
0008-6223/$ - see front matter
doi:10.1016/j.carbon.2011.06.095

exploration about potential improvements of polymer composites, (2) the high cost of carbon nanofillers. Thus, improving the dispersion of carbon nanofillers in polymeric matrices and reducing the quantity of nanofillers are critical issues for the application of polymer composites with carbon nanofillers.

Recently, graphene nanosheet (GNS), a single layer of hexagonally arrayed sp^2-bonded carbon atom, has been attractive due to the quantum Hall effect [10], ambipolar electric field [11], superior mechanical [12], electrical [13] and thermal [14] properties. It has been expected as the promising reinforcement for polymer composites because of its extremely high aspect ratio, unique graphitized plane structure, and low manufacturing cost. The GNS planar structure can provide a 2-D path for phonon transport, and the ultrahigh surface area of GNS allows a large contact area with polymer resulting in better enhancement of composite thermal conductivity than carbon nanotubes (CNTs) [15]. The conventional method for preparing graphene sheets is the reduction of graphite oxide (GO) prepared from chemical oxidation of graphite [16]. The chemically derived GO consists of a small number of aromatic segments with unoxidized benzene rings and a large number of segments containing aliphatic six membered rings, resulting in poor electrical and thermal conductivity [17]. In order to restore the structure of GNS, researchers have proposed many methods to reduce GO to GNS, such as chemical conversion with various reducing agents, electrochemical reduction, hydrothermal reduction and thermal exfoliation [18–22]. Among these methods, the thermal reduction has been widely used owing to the high efficiency of GO reduction and the advantage of bulk production [23].

Although highly reduced GO can be obtained through thermal reduction, the GNS would easily aggregate and restack due to strong Van der Waals interaction among individual GNS. Since the physicochemical properties of aggregated GS are similar to graphite, on the basis of previous literature, its reinforcing performances on polymer matrix are not as good as expected [24,25]. There are several alternative approaches to improve the solubility of GNS in solvent, which is similar to the modification of carbon nanotubes. The GNS can be readily functionalized via covalent C—C coupling reactions which derivate graphene with different organic moieties needed for the processing of polymer composites. The grafting of polymers on graphene sheets could provide good dispersion and enhance strength/conductivity properties with bulk materials [26–28]. However, the functionalization of graphene sheets led to the production of defect sites within the conjugated graphene sheet structure, which decreased the conjugation within the graphene sheets, causing significant decrease on the inherent electrical and thermal conductivity. In terms of the above reasons, the non-covalent functionalizations can be a good approach to functionalize GNS since this approach is based on Van der Waals force or π–π interaction of aromatic molecules on the GNS basal plane, which can avoid generating defects and disrupting the conjugation on the graphene surface [29–34].

In this study, an effective protocol was used to improve the thermal conductivity of GNS-filled epoxy composites through non-covalent functionalization of pyrene molecule with a functional segmented poly(glycidyl methacrylate) (Py-PGMA) on the thermally exfoliated graphene. The Py-PGMA was prepared by atomic transfer radical polymerization, which possesses the reactive pendant oxirane rings to improve the compatibility between GNS and epoxy matrix. Consequently, the Py-PGMA on GNS surface plays an important role that in inhibiting the aggregation of GNS and enhancing the interfacial interaction between GNS and polymer matrix. Furthermore, Py-PGMA that was functionalized on GNS can facilitate GNS to disperse in polymer composites homogeneously, increasing contact surface area between Py-PGMA–GNS and the polymer. This study also investigated the reinforcing efficiency of carbon nanotubes, GO, thermal exfoliated graphene, and Py-PGMA modified graphene in the thermal conductivity of polymer composites. Moreover, the thermal conductivity of Py-PGMA–GNS/epoxy composites could be enormously increased with only 4 phr graphene loading.

2. Experimental

2.1. Materials

Glycidyl methacrylate (GMA, 97%), triethylamine (TEA, 99%) and calcium hydride were purchased from Acros Organic Co., Belgium. 2-Bromopropionyl bromide (97%), copper(I) bromide (CuBr, 98%), 2,2′-bipyridine (bpy, 97%) and 1-pyrenemethanol (Py-OH, 98%) were obtained from Aldrich Co., USA. All solvents for synthesis of pyrene-end poly(glycidyl methacrylate) were spectrophotometry/HPLC grades or they were purified by calcium hydride and distilled under reduced pressure. Graphite flakes were obtained from Alfa Aesar Co., USA. The purity of the graphite was 99.98%. Multi-walled carbon nanotubes (MWCNTs) were produced by CVD process and were supplied by the CNT Company, Korea. The purity of the MWCNTs was 93%. The diameter of the MWCNTs was 10–50 nm; the length was 1–10 μm. The diglycidyl ether of bisphenol A (DGEBA) epoxy NPEL-128 was supplied by the Nan Ya Plastics Co. Ltd., Taiwan, with an epoxide equivalent weight of 190 g/equiv. 4,4-Diaminodiphenyl sulfone (DDS) acted as a curing agent and was supplied by Chriskev Company, Inc., USA.

2.2. Synthesis of pyrene-functional initiator (Py–Br)

2-Bromoisobutylryl bromide (5.37 mL, 43.4 mmol) was added dropwise to a stirring mixture of 1-pyrenemethanol (5.0 g, 21.5 mmol) and triethylamine (6.02 mL, 42.8 mmol) in 50 mL of tetrahydrofurane (THF) under argon in an ice bath for 1 h. After adding the acid bromide, the mixture was stirred at room temperature for 24 h. The mixture was washed with water (3 × 150 mL) and then dried with $MgSO_4$. After filtration, the mixture was recrystallized from 10-fold methanol for purification. The resulting product of Py–Br was filtrated and dried overnight at room temperature under vacuum to obtain a slightly brown powder (The synthesis method is illustrated in Fig. 1).

2.3. Synthesis of pyrene-end poly(glycidyl methacrylate) (Py-PGMA)

A polymerization protocol is as follows: Py–Br (76 mg, 0.2 mmol), GMA (2.84 g, 20 mmol, target DP of 100), bpy

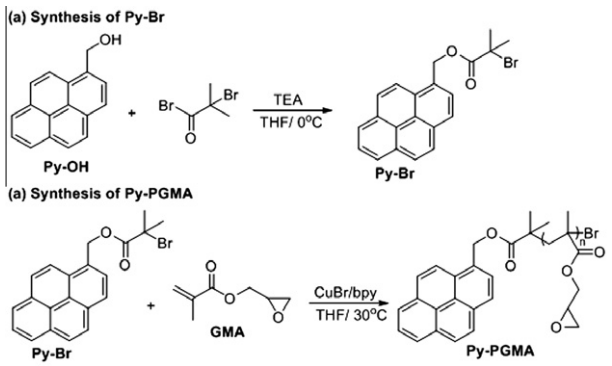

Fig. 1 – Synthesis of (a) Py–Br initiator and (b) Py-PGMA polymer.

(0.075 g, 0.48 mmol) and anhydrous ethyl acetate (3.5 mL) were added in a 25 mL round-bottom flask, and purged with nitrogen gas for 30 min. CuBr (0.035 g, 0.24 mmol) was added in a flask in nitrogen atmosphere under stirring at 30 °C. The mixture immediately became dark brown, indicating the formation of metal complex, Cu(I)Br(bpy)$_2$, which could catalyze polymerization. After 24 h, the mixture was diluted with THF, followed by passing through a silica gel column to remove the copper catalysts. The solution was condensed by rotary evaporation. Py-PGMA was precipitated from excess petroleum ether and dried in vacuum (Fig. 1). The weight of Py-PGMA was 1.6 g and the final yield was 81%. The weight average (M_w) and number average (M_n) molecular weight of Py-PGMA were determined by gel permeation chromatography (GPC), which are 7715 and 8421 g/mol, respectively. The polydispersity index (PDI) of Py-PGMA is 1.09.

2.4. *Preparation of graphene nanosheets*

The modified Hummers method [35] was conducted to oxidize graphite flakes (325 mesh) for the synthesis of GO. Ten gram of graphite flake was stirred for 7 days in a solution of 50 g potassium permanganate ($KMnO_4$) in concentrated H_2SO_4 and HNO_3 (the weight ratio of H_2SO_4 to HNO_3 is 4:1), and then reacted with H_2O_2 and washed with 5 wt.% aqueous hydrochloric acid solution to complete the oxidation and to remove the sulfate ions. The washing procedures and centrifugation of the suspension were treated repeatedly with deionized water until the solution is neutral. The GO was vacuum dried at room temperature to obtain brown powder. After GO was dried, the sample was flushed with inert gas (argon) for 10 min, and the quartz tube was quickly inserted into a furnace preheated to 1000 °C and held in the furnace for 1 min [23] (as shown in Fig. 2).

2.5. *Preparation of Py-PGMA–graphene by π–π stacking*

The weight ratio of Py-PGMA to GNS is 1:1. Py-PGMA was dissolved in acetone, followed by sonication for 30 min with adding GNS. Py-PGMA was absorbed by GNS through physical absorptions such as π–π stacking. The Py-PGMA–graphene suspension was diluted with acetone and filtered with a Nylon filter (0.2 μm), and dried at room temperature in a vacuum oven to obtain Py-PGMA–GNS (as illustrated in Fig. 2).

2.6. *Preparation of graphene/epoxy and (multi-walled carbon nanotubes) MWCNT/epoxy composites*

The mole ratio of epoxy to DDS, 1:0.5, is used to prepare the MWCNTs/epoxy and GNS/epoxy composites. Graphene and MWCNT with DDS were dispersed in acetone by an

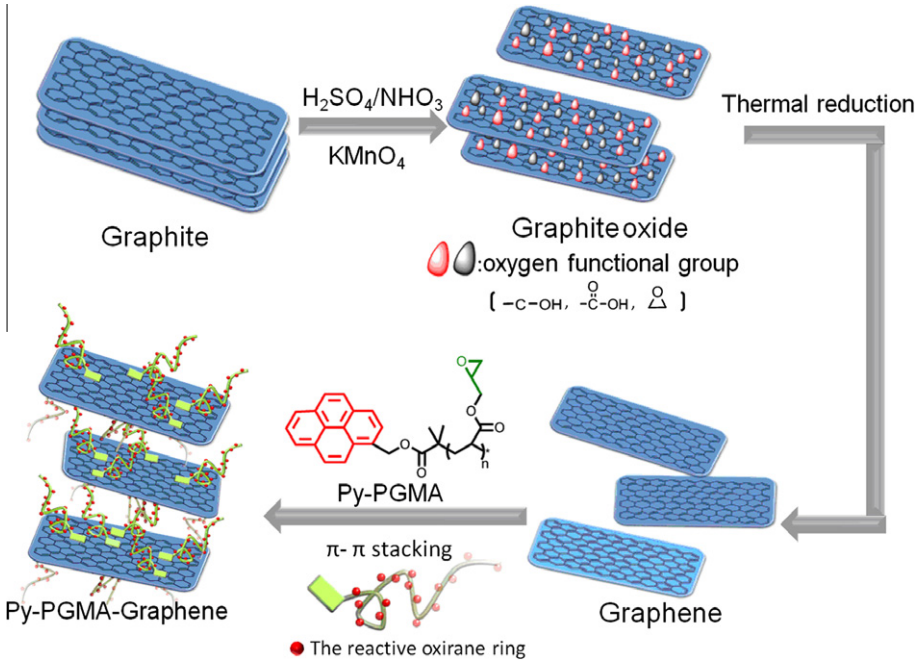

Fig. 2 – The schematic diagram of the preparation of graphene and functionalization of graphene.

ultrasonicator bath for 10 min. Then epoxy resin and reform agent were added and the slurry was stirred for 10 min to obtain good homogeneity. The mixture was transferred to a mold and degassed in a vacuum oven at 60 °C until all solvents were evacuated. The curing condition was 1 h at 60 °C, 4 h at 120 °C, 2 h at 160 °C, and 2 h at 180 °C.

2.7. Characterization and instruments

X-ray diffraction (XRD) measurements were conducted at room temperature at a scan rate of 2 min^{-1} using a Shimadzu XD-5 X-ray diffractor (40 kV, 20 mA, $\lambda = 0.1542$ nm) with copper target and Ni filter. X-ray photoelectron spectra (XPS) measurements were performed by a PHI Quantera SXM/AES 650 Auger Electron Spectrometer (ULVAC-PHI, Inc.) equipped with a hemispherical electron analyzer and a scanning monochromated Al Kα ($h\upsilon = 1486.6$ eV) X-ray source. A small spot lens system was allowed to analyze the sample that was less than 1 mm^2 in area. Raman spectra were recorded with LabRam I confocal Raman spectrometer (Dilor). The excitation wavelength was 633 nm from He–Ne laser with a laser power of ca. 15 mW at the sample surface. Thermogravimetric analysis (TGA) was conducted by Perkin-Elmer Pyris 1 with a heating rate of 10 °C min^{-1} under N_2 atmosphere. The thermal conductivity was measured by a Hot Disk thermal analyzer (TPS2500), based upon the TPS method [36]. The dimension of bulk specimens is $50 \times 50 \times 4$ mm with the sensor placed between two similar slabs of materials. The senor supplied a heat pulse of 0.08 W for 5 s to the sample and associated change in temperature which was recorded. The thermal conductivity of the samples was obtained by fitting the data according to Gustavsson et al. [37]. The morphology of graphene was investigated by a field emission-scanning electron microscope (FE-SEM, JEOL JSM-7000) with an accelerating potential of 15.0 kV. Transmission electron microscopy (TEM) analyses were conducted on a JEM-2100 electron microscope at 200 kV, and the samples for TEM measurements were prepared by one drop casting on lacey coated copper grids followed by solvent evaporation in air at room temperature. The thickness of graphene was identified by an atomic force microscope (AFM, Digital Instrument D3100). Thermal characterization was performed by a Q60 Differential scanning calorimeter (DSC). The curing processes of the epoxy composites were studied through non-isothermal scans on 5 mg samples.

3. Results and discussion

The structure of Py-PGMA was characterized by ^{1}H NMR spectrum, as shown in Fig. 3. The chemical shifts at $\delta = 8.30$ to 8.00 (a), 5.80 (b), and 1.26 (g) indicated the protons of the pyrene-functional initiator group with area ratios of 9.90:2.00:5.68 (a:b:c). The chemical shifts at $\delta = 0.94$, 1.09 and 1.29 ppm (h) were assigned to the protons of the methyl, which split into three peaks, i.e., isotactic, heterotactic and syndiotactic triads, respectively [38]. The chemical shift at $\delta = 1.89$ ppm (f) was attributed to the methylene group. Those chemical shifts at $\delta = 3.80$ and 4.31 ppm were assigned to the – O—CH_2-group (c). The peaks at $\delta = 3.24$ ppm (d) and $\delta = 2.63$ and 2.84 ppm (e) were assigned to the protons of the oxirane ring. Furthermore, the ratio of 3.14:1.00:2.09 for peak areas of h, d and e was close to 3:1:2. These results indicated that the epoxy groups in the PGMA remained intact throughout the polymerizations of GMA. Moreover, the average repeating units of 71 (Calculated Mn ~ 10,500 g/mol) for Py-PGMA could be obtained by the area ratios of 35.62:1.00 for protons of (c2) and (b), corresponding to Mn of 8421 g/mol by GPC analysis.

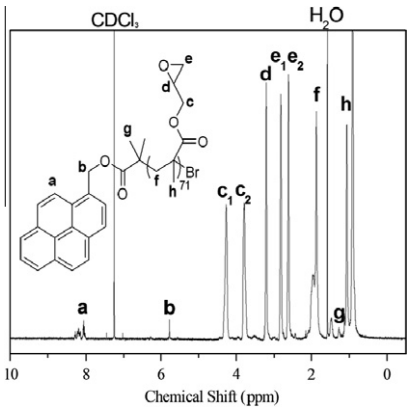

Fig. 3 – ^{1}HNMR spectrum of Py-PGMA.

The XPS spectra were analyzed to identify the surface chemical composition and variation of graphite, GO, GNS, and Py-PGMA–GNS. Fig. 4 presents the C1s core level spectra of these materials. Detailed information about the deconvoluted C1s peaks is shown in Table 1. The C1s signal of GO indicates a significant degree of oxidation, which consists of five different chemically shifted components and can be deconvoluted into: sp^2 C=C, sp^3 C—C in aromatic rings (284.6 and 284.9 eV); C—OH (285.4 eV); C—O—C (286.7 eV); C=O (287.3 eV); O—C=O (288.6 eV), respectively. These assignments agree with previous works [22,39]. Moreover, the shake-up satellite (π–π^*, 290.4 eV) assigned to π-electrons were delocalized at the aromatic network in graphite, disappearing with increasing oxidation [40]. After thermal reduction of GO, Fig. 4(c) shows a significantly decreased component for C—OH (285.5 eV), C—O—C (286.4 eV), C=O (287.5 eV), O—C=O (288.6 eV) and an increased component for C=C, C—C. The carbon sp^2 fraction of ~69% can be achieved upon thermal treatment at 1000 °C (The carbon sp^2 fraction of GO is ~29%), indicating that most of these oxygen functionalities have been removed. The π–π^* signal at 291.1 eV appeared in the graphene, which indicated that the delocalized π conjugation was restored in the graphene. Upon subsequent surface functionalization by Py-PGMA, a principal increase of the epoxide component was from 7.64% (GNS) to 20.05% (Py-PGMA–GNS), due to the presence of Py-PGMA molecules on the graphene surface.

The degree of exfoliation of GNS was characterized by X-ray diffraction (XRD). Fig. 5(a) shows the XRD spectra of pristine graphite, GO and GNS. The graphite exhibits a typical sharp (0 0 2) peak at 26.46° with an interlayer spacing of 0.337 nm. However, the peak of GO disappeared and a weak diffraction peak appeared at 8.92°, corresponding to a *d*-spacing of 0.99 nm, which implied that most oxygen atoms were bonded to the graphite planar surface as graphite transformed into GO [41]. After thermal reduction, the peak of GO

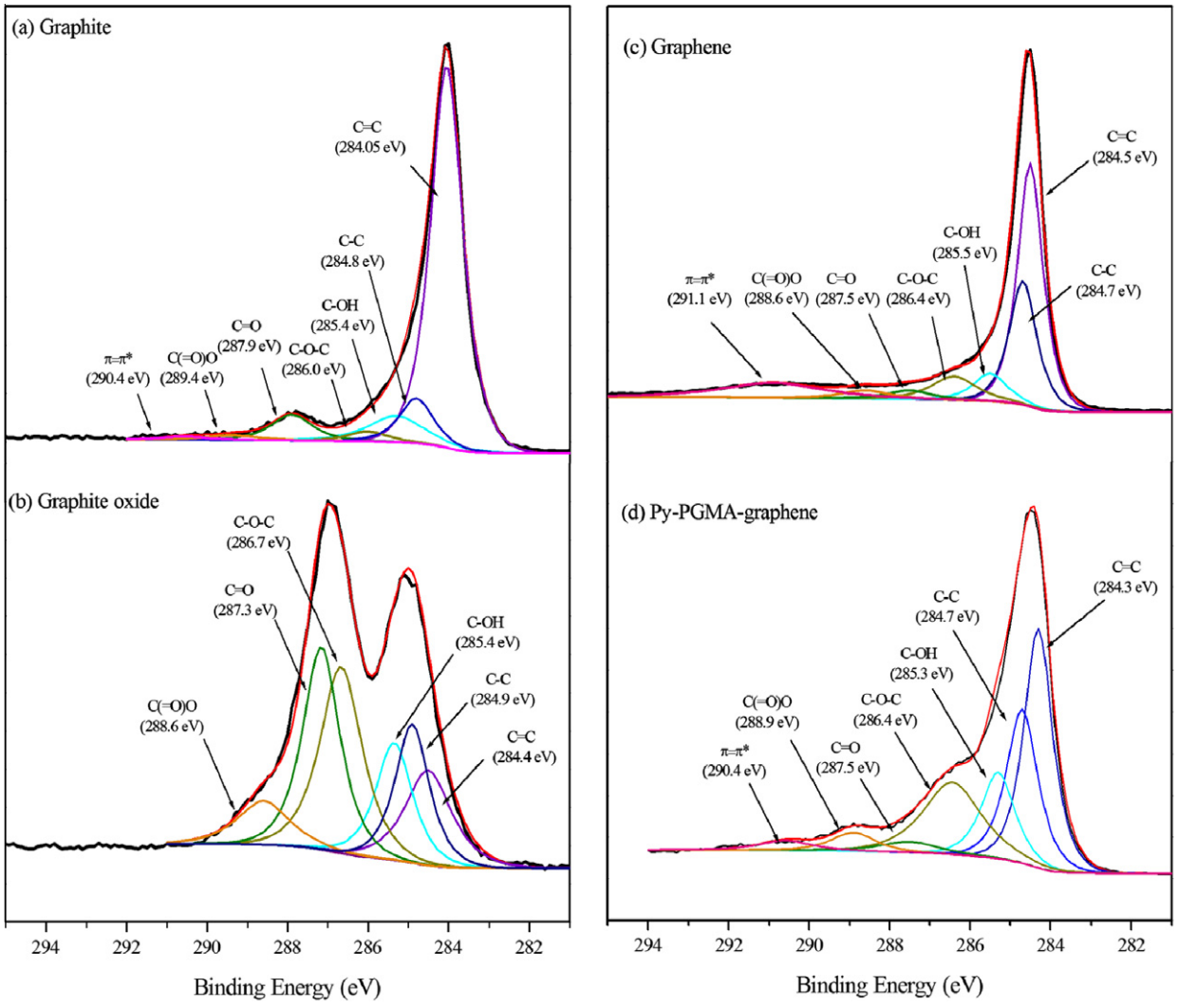

Fig. 4 – C1s XPS spectra of (a) graphite, (b) GO, (c) graphene, (d) Py-PGMA–graphene.

Table 1 – Analysis of the deconvoluted C1s peaks from XPS and their relative atomic percentage in terms of graphite, GO, graphene, and Py-PGMA–graphene.

Sample name	C1s fitting binding energy (eV; relative atomic percentage, %)					
	C=C (sp^2), C–C(sp^3)	C—OH	C—O—C	C=O	O—C=O	π–π*
XPS C1s peaks						
Graphite	284.05,284.80 (80.70)	285.30 (8.50)	286.00 (2.30)	287.90 (6.20)	289.40 (1.42)	290.40 (0.88)
Graphite oxide	284.50.284.90 (29.39)	285.35 (13.98)	286.73 (25.16)	287.23 (24.25)	288.60 (7.22)	
Graphene	284.50,284.70 (69.18)	285.50 (6.83)	286.40 (7.64)	287.50 (2.78)	288.60 (2.86)	290.90 (10.71)
Py-PGMA–graphene	284.30.284.70 (56.13)	285.30 (10.90)	286.44 (20.05)	287.50 (3.47)	288.90 (6.89)	290.45 (2.56)

at 8.92° was disappeared. This meant that a large amount of oxidized functional groups was removed from the interlayer spacing of GO and the quickly removal of oxidized functional groups leading to fast exfoliation of GNS. Fig. 5(b) shows a typical multiple Lorentzian fitting for the (0 0 2) reflection in the case of graphene, three peaks around 19.5°, 20.9° and 22.2° were fitted. These corresponded to *d*-spacing values of 0.455, 0.423 and 0.400 nm. It is noted that these peaks are lower and broader than those of the pristine graphite, which implied that the graphene forms a randomly ordered carbonaceous layered solid with a corrugated structure [42]. The corresponding layers of graphene with these three fitting peaks were calculated by Scherrer equation [43], which are around 3–6 layers.

Raman spectra of graphite, GO, GNS and functionalized GNS are shown in Fig. 6. For the pristine graphite, a couple of Raman active bands can be observed. One is the G band (in-phase vibration of the graphite lattice, E_{2g} mode) at 1575 cm^{-1}; the other is the weak D band (defects inherent in the graphite and the edge effect of graphite, A_{1g} mode) around

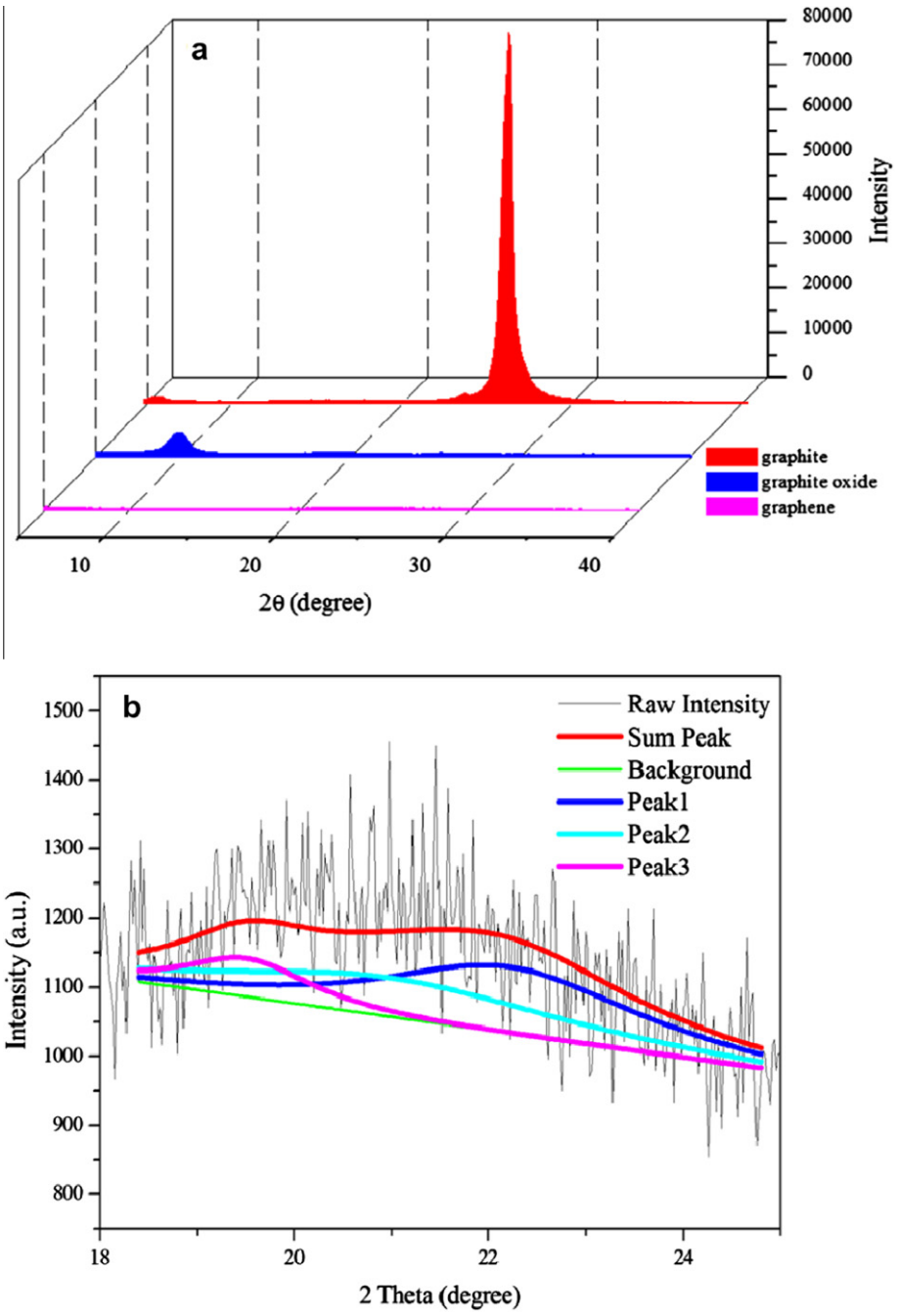

Fig. 5 – XRD patterns of (a) graphite, GO, and graphene, (b) graphene with Lorentzian fitting.

1350 cm^{-1}. The significant structure changed during the oxidation from graphite to GO; the G band was broadened and shifted to high frequency, and the D band becomes higher relative intensity. It reflected the reduction in size of the in-plane sp^2 domains. When GO transformed to graphene, the G band slightly shifted back to the location of the G band in graphite. Meanwhile, the decrease of D band intensity was attributed to graphite "self-healing" by heat reduction [44]. The current study estimated the in-plane crystallite size L_a in disordered carbon materials, since the integrated intensity ratio of G band to D band was related to L_a, $L_a = 4.4(I_G/I_D)$ [45,46]. The I_G/I_D ratio of graphite, GO, GNS, and Py-PGMA–GNS is 5.11, 0.95, 1.91, and 1.85. Hence, L_a of graphite, GO, and GNS is 22.48, 4.18, and 8.40, respectively. Graphite possesses the largest L_a, while GO has the smallest comparing to graphite and graphene. The L_a of GO was reduced from 22.48 to 4.18 by oxidation, indicating the defect density was significant. After thermal treatment, the L_a of graphene was increased from 4.18 (GO) to 8.40. Since the sp^2 sites may be isolated reduction and also has a vacancy in the lattice, their spatial distribution in the lattice does not form a continuous sp^2 phase. Noticeably, the electrical and thermal conductive properties are positive relate to large L_a of graphene-based materials. Comparing the L_a of graphene with that of

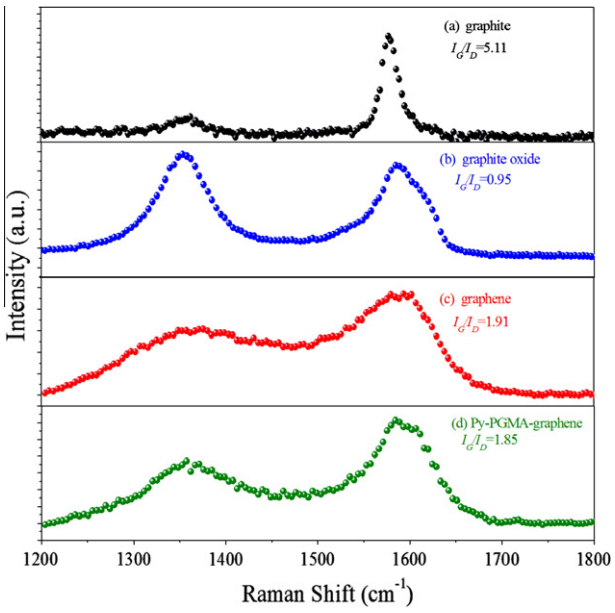

Fig. 6 – Raman spectra of graphite, GO, graphene, and Py-PGMA–graphene.

multi-walled carbon nanotubes (MWCNTs), the L_a of GNS is slightly higher than that of MWCNTs (L_a = 4.23 nm), which implies that the graphene possesses better physical properties. Particularly, the I_G/I_D ratio of Py-PGMA–GNS is slightly lower than that of graphene and higher than GO, which reveals that the non-covalent functionalization can avoid the damage to conjugated structure of GNS [33].

For further investigation about the morphology of graphene and Py-PGMA–graphene, SEM, TEM and AFM have been utilized (Fig. 7). The dimension of GNS is approximately 9 × 7 μm and exhibits the bumpy texture as found in the flat regions (Fig. 7(a)). The extremely small thickness and isolated oxygen reaction sites caused the wrinkled topology of graphene (Fig. 7(b)). Fig. 7(c) shows that dark elliptical spots on the Py-PGMA–GNS surface, which would be regarded as the morphology of the Py-PGMA. The specimen for TEM was prepared by dripping a Py-PGMA–GNS/THF solution onto a copper grid coated with a lacy carbon, and then the solvent was removed at 70 °C. Because of the speedy drying condition, Py-PGMA formed the condensed structure (elliptical spot). To assess the dispersion ability of the resulting graphene, THF solutions of the samples at 1 mg/mL was ultrasonic dispersed 10 min and then placed steady for 1 day (Fig. 7(d) insert). Py-PGMA–GNS solution showed a black and stable state, which meant

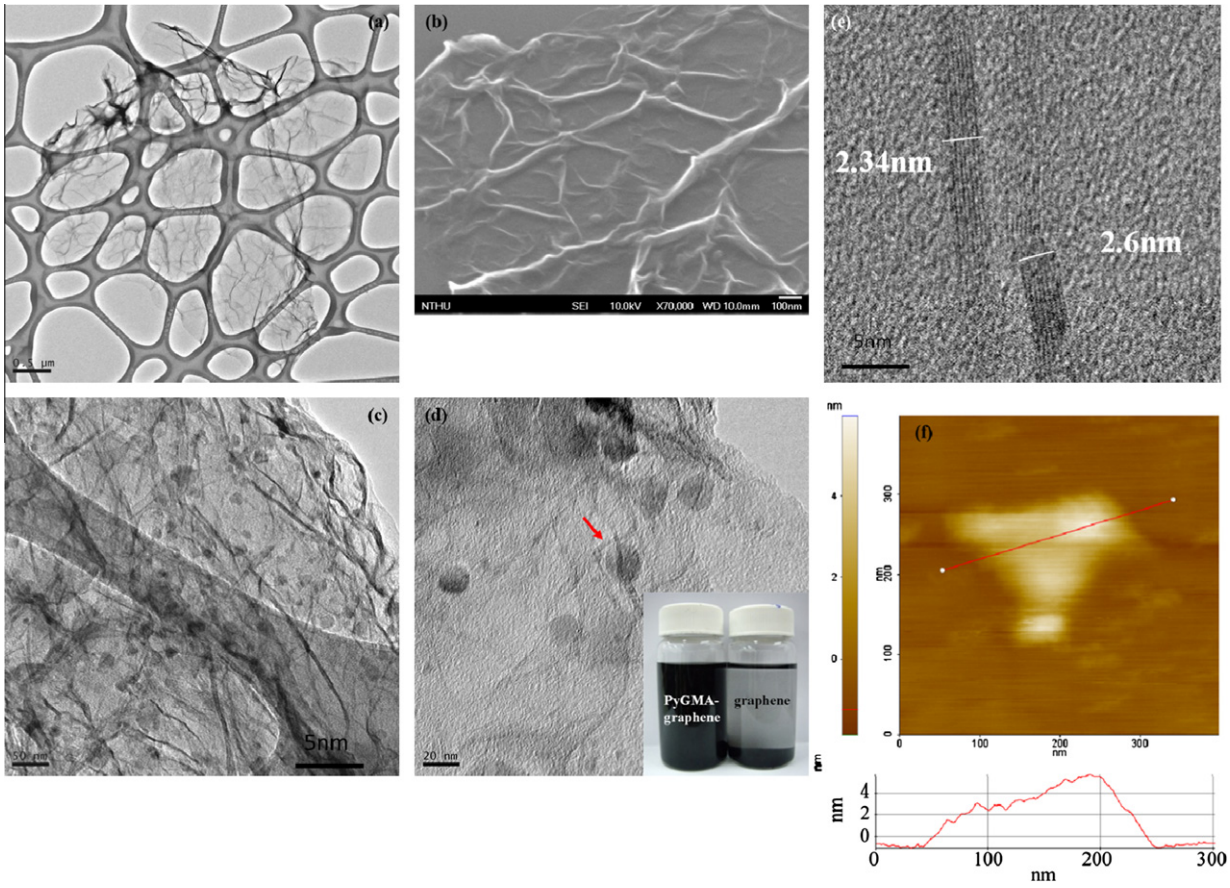

Fig. 7 – TEM images of (a) graphene, (c), (d) Py-PGMA–graphene (insert photograph of Py-PGMA–graphene and pristine graphene dispersed in THF for 1 day, respectively), and (e) Py-PGMA–graphene/epoxy composite core section. The SEM image of (b) graphene and the AFM image of (f) graphene.

that the Py-PGMA was absorbed onto graphene and the PGMA chains lead to the steric stabilization in organic solvent to overcome the strong Van der Waal forces among individual nanosheet. The number of graphene layers could be observed by the core section of Py-PGMA–GNS/epoxy composite (Fig. 7(e)), which was around seven layers, similar to the number of layers calculated from XRD. The AFM image of the GNS (Fig. 7(f)) presents that the average thickness of graphene sheet is 2.30 nm. As for the AFM image of graphene, its upper right edge is double-fold onto itself, as can be determined the thickness about 5.1 nm. These results suggested that the GNS could be prepared from GO through thermal exfoliation.

In previous study [47], TGA was utilized to investigate the thermal stability of carbonerous materials. For example, the disordered or amorphous carbons tended to be oxidized at around 500 °C due to their lower activation energies for oxidation or the presence of a large number of actives sites. However, the well graphitized structure started to oxidize at a higher temperature around 800 °C [48]. On the other hand, TGA is also a useful tool to characterize the quantity of organic substances grafted to carbonerous materials, because the organic substances covalently attached to the surface of graphene-based materials was thermally stripped off in the temperature range from 250 to 500 °C. Fig. 8 shows that GO is thermally unstable; the weight loss occurred even below 100 °C and primary weight loss of GO was approximately 200–300 °C. This resulted from the pyrolysis of oxygen containing functional groups of CO, CO_2, and steam [49]. This study suggested an increase in the thermal stability of graphene following the restore of the graphitic structure through thermal reduction. The TGA curve of Py-PGMA–GNS shows the organic content on graphene is around 26%, which reveals that the Py-PGMA attached on GNS successfully. Furthermore, the thermal stability of Py-PGMA–GNS is as good as the GNS indicating that the structure of GNS cannot be destroyed though non-covalent functionalization, which is in good agreement with the results of XPS and Raman.

The comparison of the DSC curves of epoxy composites with 0.25 phr pristine GNS and Py-PGMA–GNS could address the interfacial interaction between the epoxy matrix and the GNS. Fig. 9 shows that the enthalpy (ΔH) of 0.25 phr pristine GNS/epoxy during curing reaction is smaller than that of neat epoxy (From 128.95 J/g (neat epoxy) to 93.24 J/g (0.25 phr pristine graphene/epoxy)), and the exothermal peak temperature shifts to a higher temperature (From 205.4 °C (neat epoxy) to 211.3 °C (0.25 phr pristine graphene/epoxy)). These results confirmed the steric hindrance effect on the curing reaction, with the addition of graphene, which is due to the high surface area of nanosheet. The surface area of the graphene agglomerate was 686 m^2/g, measured by the N_2 absorption Brunauer Emmett Teller (BET) method. Therefore, the presence of graphene increased viscosity which reduced the reactivity. This phenomenon has also been observed by other systems [50,51]. However, this study shows the opposite effect when adding functionalized GNS. The ΔH of functionalized GNS/epoxy is higher than other systems, and a weak exothermal peak appears at 147 °C. This caused the reactive sites of the functionalized GNS to form a chemical linkage with the epoxy matrix during the crosslinking reaction. It also improved the interfacial interaction between epoxy and graphene. In addition, the ΔH of functionalized GNS/epoxy is higher than that of neat epoxy, which may be a result of the proportional increase of epoxide concentration in the composites.

Thermal conductivity is affected by the carbon nanofiller structure within the matrix, loading, dispersion, and the thermal resistance of the interface between nanofillers and the polymer matrix. Fig. 10 shows significant increase in the thermal conductivity of the epoxy composites with the increasing graphene content, which is superior to the MWCNT/epoxy composites. Because GNS possesses higher surface area to contact with polymer than MWCNT, the thinner polymer layer on GNS can reduce the barriers of phonon transport. By contrast, the Py-PGMA–GNS/epoxy composite exhibited the best efficiency in improvement of thermal conductivity, compared with epoxy composites with MWCNTs or GNS. Thermal conductivity of 1 phr Py-PGMA–GNS/epoxy composites increased about 16.4%, compared with that of 1 phr pristine GNS/epoxy; on the other hand, thermal conductivity of

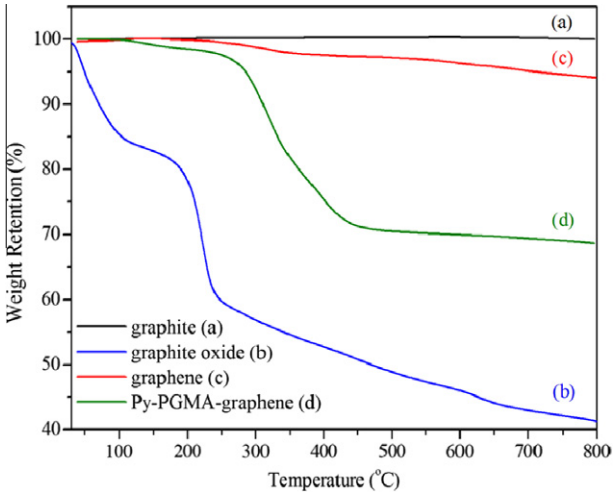

Fig. 8 – TGA thermograms of graphite, graphite oxide, graphene, and Py-PGMA–graphene.

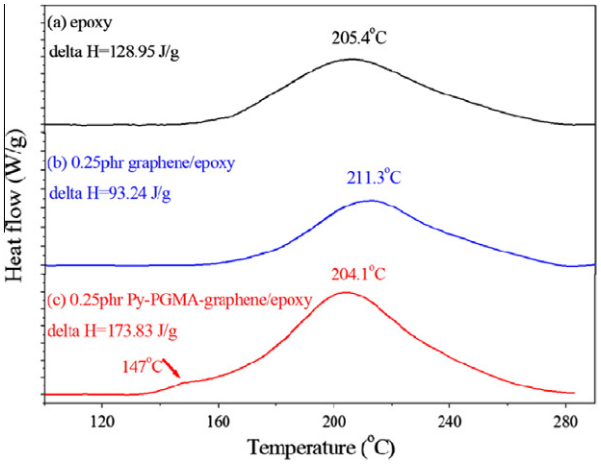

Fig. 9 – DSC curves of (a) epoxy, (b) 0.25 phr graphene/epoxy, and (c) 0.25 phr Py-PGMA–graphene.

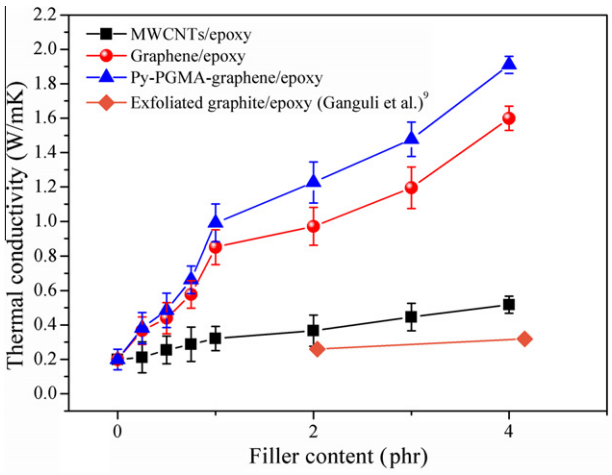

Fig. 10 – Thermal conductivity with various filler contents of MWCNTs/epoxy, graphene/epoxy, and Py-PGMA–graphene.

1 phr Py-PGMA–GNS/epoxy composites about 208.7%, being much higher than that of 1 phr pristine MWCNTs. It was noticeable that the thermal conductivity of Py-PGMA–GNS/epoxy with only 4 phr loading reached 1.91 W/mK; it usually required about 20 times graphite content (80–200 phr) to achieve the comparable thermal conductivities. Three reasons were proposed to explain this significant enhancement: (i) the better graphitic integrity of GNS can possess better conductance. The XPS and Raman results revealed that thermal exfoliation could reduce GO efficiently, and Py-PGMA modified GNS through non-covalent functionalization can preserve the structure integrity of GNS; (ii) the DSC analysis indicated that the functional groups on Py-PGMA–GNS could generate covalent bonds with epoxy matrix, and further formed the cross-linked structure of Py-PGMA–graphene/epoxy composites, which could enhance the interfacial interaction between GNS and epoxy considerably. The strong interaction between nanofillers and polymer could reduce the thermal interfacial resistance effectively and improve the phonon transport in composite; (iii) the excellent solubility of Py-PGMA modified GNS in solvent can facilitate GNS to disperse in polymer composites homogeneously, resulting in an increased contact surface area between Py-PGMA–GNS and the polymer. The homogeneous Py-PGMA–GNS possess a large contact area with polymer permitting ease of heat flows and promoting phonon diffusion in Py-PGMA–GNS/epoxy composites.

In summary, the theoretic performance of GNS would be reduced significantly due to the nanosheet aggregation and poor compatibility with polymer, which is the critical issue in relation to the potential of GNS in polymer composites. Consequently, pyrene molecule with functional segmented polymer chain can be a good approach to improve the performance of GNS in polymer composite though non-covalent functionalization.

4. Conclusions

This study demonstrated a non-destructive approach to improve the thermal conductivity of GNS-filled epoxy composites through non-covalent functionalization of pyrene molecules with a functional segmented polymer chain on the thermally exfoliated graphene. The thermal conductivity of Py-PGMA–GNS/epoxy composite increased more than 800% with low GNS loading (4 phr), compared with neat epoxy, which was superior to the epoxy composites with individual MWCNTs or GNS. At loading 4 phr Py-PGMA–GNS has about 20% higher thermal conductivity than pristine GNS. The remarkable improvement originated from the Py-PGMA functionalization. The Py-PGMA on GNS surface plays an important role in inhibiting their aggregation and facilitating dispersion within polymer matrix homogeneously. Furthermore, Py-PGMA on GNS could generate covalent bonds with the epoxy to form a cross-linked structure of Py-PGMA–GNS/epoxy composites; the integrated Py-PGMA–GNS/epoxy composite can possess a large contact area with polymer permitting ease of heat flows and promoting phonon diffusion. Consequently, the non-destructive approach can maintain the high graphitic integrity of GNS and improve the GNS-epoxy interaction, which is of critical importance for the potential of graphene-based materials in enhancing thermal conductivity of polymer-based composite.

Acknowledgment

The financial support from the Industrial Technology Research Institute and National Science Council of Taiwan ROC under contract no. NSC-99-2221-E-007-005 and the boost program of the Low Carbon Energy Research Center of National Tsing Hua University, are gratefully acknowledged.

REFERENCES

[1] Coleman JN, Khan U, Blau WJ, Gunko YK. Small but strong: a review of the mechanical properties of carbon nanotubes–polymer composites. Carbon 2006;44:1624–52.
[4] Hong J, Lee J, Jung D, Shim SE. Thermal and electrical conduction behavior of alumina and multiwalled carbon nanotubes incorporated poly(dimethyl siloxane). Thermochim Acta 2011;512:34–9.
[5] Zhou W, Qi S, Li H, Shao S. Study on insulating thermal conductive BN/HDPE composites. Carbon 2010;48:1171–6.
[6] Yu S, Hing P, Hu X. Thermal conductivity of polystyrene–aluminum nitride composite. Compos Part A 2002;33:289–92.
[7] Veca LM, Meziani MJ, Wang W, Wang X, Lu F, Zhang P, et al. Carbon nanosheets for polymeric nanocomposites with high thermal conductivity. Adv Mater 2009;21:2088–92.
[8] Yu A, Ramesh P, Sun X, Bekyarova E, Itkis ME, et al. Enhanced thermal conductivity in a hybrid graphite nanoplatelet-carbon nanotubes filler for epoxy composites. Adv Mater 2008;20:4740–4.
[9] Ganguli S, Roy AK, Anderson DP. Improved thermal conductivity for chemically functionalized exfoliated graphite/epoxy composites. Carbon 2008;46:806–17.
[10] Novoselov KS, Jiang Z, Morozov SV, Stormer HL, Zeitler U, Maan JC, et al. Room-temperature quantum hall effect in graphene. Science 2007;315:1379.
[11] Novoselov KS, Geim AK, Morozov SV, Jiang D, Zhang Y, Dubonos SV, et al. Electric field effect in atomically thin carbon films. Science 2004;306:666–9.

[12] Gómez-Navarro C, Burghard M, Kern K. Elastic properties of chemically derived single graphene sheets. Nano Lett 2008;8:2045–9.
[13] Novoselov KS, Morozov SV, Mohinddin TMG, Ponomarenko LA, Elias DC, Yang R, et al. Electronic properties of graphene. Phys Status Solidi B 2007;244:4106–11.
[14] Yu A, Ramesh P, Itkis M E, Bekyarova E, Haddon R C. Graphite nanoplatelet-epoxy composites thermal interface materials. J Phys Chem C 2007;111:7565–9.
[15] Balandin AA, Ghosh S, Bao W, Calizo I, Teweldebrhan D, Miao F, et al. Superior thermal conductivity of single-layer graphene. Nano Lett 2008;8:902–7.
[16] Lerf A, He H, Forster M, Klinowski J. Structure of graphite oxide revisited. J Phys Chem B 1998;102:4477–82.
[17] Yang D, Velamakanni A, Bozoklu G, Park S, Stoller M, Piner RD. Chemical analysis of graphene oxide films after heat and chemical treatments by X-ray photoelectron and micro-raman spectroscopy. Carbon 2009;47:145–52.
[18] Zhang T, Zhang D, Shen M. A low-cost method for preliminary separation of reduced graphene oxide nanosheets. Mater Lett 2009;63:2051–4.
[19] Ju HM, Huh SH, Choi SH, Lee HL. Structures of thermally and chemically reduced graphene. Mater Lett 2010;64:357–60.
[20] Lee KR, Lee KU, Lee JW, Ahn BT, Woo SI. Electrochemical oxygen reduction on nitrogen doped graphene sheets in acid media. Electrochem Commun 2010;12:1052–5.
[21] Nethravathi C, Rajamathi M. Chemically modified graphene sheets produced by the solvothermal reduction of colloidal dispersions of graphite oxide. Carbon 2008;46:1994–8.
[22] Park S, Ruoff RS. Chemical methods for the production of graphene. Nat Nanotechnol 2009;4:217–24.
[23] Mcallister MJ, Li LJ, Adamson DH, Schniepp HC, Abdala AA, Liu J, et al. Single sheet functionalized graphene by oxidation and thermal expansion of graphite. Chem Mater 2007;19:4396–404.
[24] Stankovich S, Piner RD, Nguyen ST, Ruoff RS. Synthesis and exfoliation of isocyanate-treated graphene oxide nanoplatelets. Carbon 2006;44:3342–7.
[25] Xu Y, Bai H, Lu G, Li C, Shi G. Flexible graphene films via the filtration of water-soluble noncovalent functionalized graphene sheets. J Am Chem Soc 2008;130:5856–7.
[26] Fang M, Wang K, Lu H, Yang Y, Nutt S. Covalent polymer functionalization of graphene nanosheets and mechanical properties of composites. J Mater Chem 2009;19:7098–105.
[27] Fang M, Wang K, Lu H, Yang Y, Nutt S. Single-layer graphene nanosheets with controlled grafting of polymer chains. J Mater Chem 2010;20:1982–92.
[28] Fang M, Zhang Z, Li J, Zhang H, Lu H, Yang Y. Constructing hierarchically structured interphases for strong and tough epoxy nanocomposites by amine-rich graphene surfaces. J Mater Chem 2010;20:9635–43.
[29] Bahun GJ, Wang C, Adronov A. Solubilizing single-walled carbon nanotubes with pyrene-functionalized block copolymers. J Polym Sci A 2006;44:1941–51.
[30] Choi I H, Park M, Lee SS, Hong SC. Pyrene-containing polystyrene segmented copolymer from nitroxide mediated polymerization and its application for the noncovalent functionalization of as-prepared multiwalled carbon nanotubes. Eur Polym J 2008;44:3087–95.
[31] Lou X, Daussin R, Cuenot S, Duwez AS, Pagnoulle C, Detrembleur C, et al. Synthesis of pyrene-containing polymers and noncovalent sidewall functionalization of multiwalled carbon nanotubes. Chem Mater 2004;16:4005–11.
[32] Cosnier S, Holzinger M. Design of carbon nanotubes–polymer frameworks by electropolymerization of single-walled carbon nanotube-pyrrole derivatives. Electrochim Acta 2008;53:3948–54.
[33] Yang Q, Pan X, Huang F, Li K. Fabrication of high-concentration and stable aqueous suspensions of graphene nanosheets by noncovalent functionalization with lignin and cellulose derivatives. J Phys Chem C 2010;114:3811–6.
[34] Meuer S, Braun L, Schilling T, Zentel R. α-Pyrene polymer functionalized multiwalled carbon nanotubes: solubility, stability and depletion phenomena. Polymer 2009;50:154–60.
[35] Hummers W, Offeman R. Preparation of graphitic oxide. J Am Chem Soc 1958;80:1339.
[36] Zhu D, Li X, Wang N, Wang X, Gao J, Li H. Dispersion behavior and thermal conductivity characteristics of Al_2O_3–H_2O nanofluids. Curr Appl Phys 2009;9:131–9.
[37] Gustavsson M, Karawacki E, Gustafsson SE. Thermal conductivity, thermal diffusivity, and specific heat of thin samples from transient measurements with hot disk sensors. Rev Sci Instrum 1994;65:3856–60.
[38] Li G, Zhu X, Zhu J, Cheng Z, Zhang W. Homogeneous reverse atom transfer radical polymerization of glycidyl methacrylate and ring-opening reaction of the pendant oxirane ring. Polymer 2005;46:12716–21.
[39] Park S, Lee KS, Bozoklu G, Cai W, Nguyen ST, Ruoff RS. Graphene oxide papers modified by divalent ions-enhancing mechanical properties via chemical cross-linking. ACS Nano 2008;2:572–8.
[40] Hontoria-Lucas C, Lpez-Peinado AJ, Lpez-González JDD, Rojas-Cervantes ML, Martín-Aranda RM. Study of oxygen-containing groups in a series of graphite oxides: physical and chemical characterization. Carbon 1995;33:1585–92.
[41] Lv W, Tang DM, He YB, You CH, Shi ZQ, Chen XC, et al. Low-temperature exfoliated graphenes: vacuum-promoted exfoliation and electrochemical energy storage. ACS Nano 2009;3:3730–6.
[42] Shen J, Hu Y, Shi M, Lu X, Qin C, Li C, et al. Fast and facile preparation of graphene oxide and reduced graphene oxide nanoplatelets. Chem Mater 2009;21:3514–20.
[43] Tanaka R, Sato E, Hunt JE, Winans RE, Sato S, Takanohashi T. Characterization of asphaltene aggregates using X-ray diffraction and small angle X-ray scattering. Energy Fuels 2004;18:1118–25.
[44] Kudin KN, Ozbas B, Schniepp HC, Prud'homme RK, Aksay IA, Car R. Raman spectra of graphite oxide and functionalized graphene sheets. Nano Lett 2008;8:36–41.
[45] Sato K, Saito R, Oyama Y, Jiang J, Cancado LG, Pimenta MA, et al. D-band Raman intensity of graphitic materials as a function of laser energy and crystallite size. Chem Phys Lett 2006;427:117–21.
[46] Subrahmanyam KS, Vivekchand SRC, Govindaraj A, Rao CNR. A study of graphene prepared by different methods: characterization, properties and solubilization. J Mater Chem 2008;18:1517–23.
[47] Wu Z S, Ren W, Gao L, Zhao J, Chen Z, Liu B, et al. Synthesis of graphene sheets with high electrical conductivity and good thermal stability by hydrogen arc discharge exfoliation. ACS Nano 2009;3:411–7.
[48] Stankovich S, Sikin DA, Piner RD, Kohlhaas KM, Kleinhammes A, Jia T, et al. Synthesis of graphene-based nanosheets via chemical reduction of exfoliated graphite oxide. Carbon 2007;45:1558–65.
[49] Shen J, Hu Y, Li C, Qin C, Ye M. Synthesis of amphiphilic graphene nanoplatelets. Small 2009;5:82–5.
[50] Abdalla M, Dean D, Robinson P, Nyairo E. Cure behavior of epoxy/MWCNT nanocomposites: the effect of nanotubes surface modification. Polymer 2008;49:3310–7.
[51] Liu D, Shi Z, Matsunaga M, Yin J. DSC investigation of the hindered effect on curing behavior for epoxy-phenol/MMT nanocomposites based on the acidic octadecylamine modifier. Polymer 2006;47:2918–27.